JOURNAL OF MOLECULAR SPECTROSCOPY 171, 169–188 (1995)

High-Resolution Fourier Transform Emission Spectroscopy of the $C^1\Sigma^+$–$X^1\Sigma^+$ and $e^3\Phi$–$a^3\Delta$ Systems of YD

R. S. RAM AND P. F. BERNATH

Department of Chemistry, University of Arizona, Tucson, Arizona 85721; and Department of Chemistry, University of Waterloo, Waterloo, Ontario, Canada N2L 3G1

High-resolution electronic emission spectra of YD have been recorded in the 690 nm to 3 μm spectral region using a Fourier transform spectrometer. YD molecules were excited in a yttrium hollow cathode lamp operated with neon gas and a trace of deuterium. The observed bands have been classified into two different electronic transitions: $C^1\Sigma^+$–$X^1\Sigma^+$ and $e^3\Phi$–$a^3\Delta$. The rotational analysis of the 0–0, 1–1, 2–2, 0–1, 1–2, and 2–3 bands of the $C^1\Sigma^+$–$X^1\Sigma^+$ system provides the following set of equilibrium molecular constants for the ground state:

$$\omega_e = 1089.1182(81)\ \text{cm}^{-1},\quad \omega_e x_e = 9.8459(38)\ \text{cm}^{-1},\quad \omega_e y_e = 0.0144(8)\ \text{cm}^{-1}$$

$$B_e = 2.320192(10)\ \text{cm}^{-1},\quad \alpha_e = 0.032960(6)\ \text{cm}^{-1},\quad \text{and } r_e = 1.920404(4)\ \text{Å}.$$

Three bands observed in the red region with origins at 11 398.0507(14), 11 523.0523(13), and 11 611.6396(7) cm^{-1} have been assigned as the 0–0 bands of the $^3\Phi_2$–$^3\Delta_1$, $^3\Phi_3$–$^3\Delta_2$, and $^3\Phi_4$–$^3\Delta_3$ subbands, respectively, of a new $e^3\Phi$–$a^3\Delta$ electronic transition. Several additional bands, all degraded toward higher wavenumbers, have been identified in the 7800–8500 cm^{-1} region. The very weak intensity of these bands limited the information which could be extracted from them.

INTRODUCTION

The electronic structure of transition metal hydrides have been subject of numerous theoretical and experimental studies (*1–9*). Theoretical ab initio studies have focussed on the characterization of the low-lying electronic states of these species and on the understanding of the metal–hydrogen bond. Molecules for which ab initio studies are available include, for example, PtH (*10*), PdH (*11–13*), YH (*14, 15*), ZrH (*16*), MoH (*17*), TiH (*18*), and ScH (*19–21*).

Some of the transition metal hydrides are found in the spectra of cool stars due to the relatively high cosmic abundance of the transition metal elements. For example, TiH (*22*) has been identified in the spectra of M-type stars; NiH (*23*) and CrH (*24*) have been seen in the spectra of sunspots. The previous work on the optical spectroscopy of transition metal hydrides have been reviewed by several groups (*1–5*). However, only limited studies are available for the corresponding deuterides.

In the visible region, the electronic spectra of many transition metal hydrides are found to be very complex due to presence of a number of close-lying electronic states, further complicated by substantial spin–orbit interactions. Therefore, the different spin components are frequently affected by strong perturbations making the interpretation of the spectra difficult. In the near-infrared region, however, the density of electronic states is expected to be much lower than that in the visible region. Thus the near-infrared spectra of these species should be relatively free from perturbations.

0022-2852/95 $6.00

TABLE I

Observed Wavenumbers (in cm^{-1}) of the $C^1\Sigma^+$–$X^1\Sigma^+$ System of YD

	0-0				1-1				2-2			
J	R(J)	O-C	P(J)	O-C	R(J)	O-C	P(J)	O-C	R(J)	O-C	P(J)	O-C
1	14330.758	-0					14158.674	-4				
2	14334.340	12	14313.015	-0	14174.980	-4	14153.822	-5	14061.410	-3		
3	14337.546	-3	14307.715	-5	14178.276	-2	14148.665	-1	14064.595	-2		
4	14340.419	-2	14302.076	-5	14181.255	1	14143.198	-1	14067.455	1	14030.088	-1
5	14342.941	0	14296.099	-2	14183.911	0	14137.422	-1	14069.985	2	14024.336	0
6	14345.113	4	14289.779	-1	14186.251	5	14131.338	-0	14072.186	2	14018.265	1
7	14346.924	1	14283.119	-0	14188.256	1	14124.947	0	14074.051	-1	14011.877	2
8	14348.383	0	14276.124	5	14189.939	2	14118.244	-1	14075.587	0	14005.172	1
9	14349.486	-0	14268.781	-0	14191.290	4	14111.235	1	14076.775	-12	13998.151	1
10	14350.236	5	14261.105	0	14192.303	2	14103.914	4	14077.649	-1	13990.812	-0
11	14350.632	15	14253.091	1	14192.980	4	14096.277	2	14078.180	6	13983.156	-2
12			14244.739	-0	14193.302	-6	14088.327	3	14078.355	-1	13975.187	-2
13	14350.301	-2	14236.053	1	14193.302	9	14080.060	2	14078.180	-14	13966.901	-1
14	14349.605	4	14227.029	1	14192.925	-1	14071.475	2	14077.530	* -158	13958.297	-2
15	14348.535	3	14217.670	1	14192.200	-4	14062.569	0	14077.009	* 174	13949.376	-2
16	14347.100	3	14207.975	1	14191.114	-10	14053.339	-1	14076.775	* 1140	13939.981	* -161
17	14345.292	0	14197.945	1	14189.607	* -70	14043.785	-4	14073.904	* -183	13930.766	* 176
18	14343.117	1	14187.581	1	14187.883	* 20	14033.899	-10	14072.105	* -89	13921.852	* 1129
19	14340.569	1	14176.881	2	14185.684	7	14023.629	* -70	14069.910	* -47	13910.360	* -182
20	13337.644	-0	14165.846	1	14183.116	3	14013.176	* 19	14067.358	* -23	13899.964	* -88
21	14334.340	-4	14154.476	0	14180.165	-3	14002.288	7	14064.467	-6	13889.207	* -49
22	14330.662	-4	14142.772	-0	14176.840	2	13991.070	3	14061.250	5	13878.137	* -25
23	14326.600	-8	14130.733	-0	14173.117	-2	13979.515	1	14057.716	9	13866.771	-6
24	14322.172	4	14118.360	-1	14169.002	-5	13967.620	-0	14053.878	-1	13855.120	6
25	14317.344	0	14105.646	-7	14164.496	-1	13955.381	-1	14049.783	-3	13843.197	10
26	14312.136	3	14092.614	4	14159.587	-1	13942.797	-0	14045.447	-8	13831.022	5
27	14306.534	-0	14079.233	1	14154.276	0	13929.865	-0	14040.932	5	13818.627	-3
28	14300.546	0	14065.519	0	14148.557	2	13916.581	-1			13806.050	-7

Note. O − C: observed-calculated line positions in units of 10^{-3} cm^{-1}; *indicates perturbed transitions not included in the fit.

TABLE I—*Continued*

	0-0				1-1				2-2			
J	R(J)	O-C	P(J)	O-C	R(J)	O-C	P(J)	O-C	R(J)	O-C	P(J)	O-C
29	14294.166	0	14051.469	-0	14142.424	-1	13902.947	-1			13793.343	6
30	14287.393	1	14037.084	-0	14135.873	-8	13888.961	-1				
31	14280.222	1	14022.363	-0	14129.184 *	262	13874.617	-2				
32	14272.651	-2	14007.304	-1	14121.563 *	18	13859.915	-6				
33	14264.684	-1	13991.909	-2	14113.753	9	13845.127 *	261				
34	14256.314	-1	13976.177	-1	14105.526	6	13829.471 *	18				
35	14247.541	1	13960.106	-1	14096.874	4	13813.688	9				
36	14238.356	-3	13943.696	-1	14087.788	-1	13797.553	8				
37	14228.768	-1	13926.948	-1	14078.276	-1	13781.050	2				
38	14218.767	-1	13909.858	-1	14068.320	-7	13764.190	2				
39	14208.362	7	13892.428	-2	14057.932	-7	13746.962	-2				
40	14197.531	4	13874.655	-4	14047.111	3	13729.366	-6				
41			13856.551	5	14035.838	9	13711.406	-6				
42			13838.092	2								
43	14162.531	3	13819.290	-1								
44	14150.014	-4	13800.152	6								
45	14137.078	-1	13780.657	0								
46	14123.709	-4	13760.821	3								
47	14109.912	-2	13740.634	0								
48	14095.683	1	13720.101	1								
49	14081.013	-0	13699.215	1								
50	14065.902	-4	13677.978	-0								
51	14050.357	2	13656.391	3								
52	14034.356	-4	13634.443	-0								
53	14017.919	1	13612.142	0								
54	14001.024	-1	13589.481	-1								
55	13983.672	-6	13566.460	-3								
56	13965.882	8	13543.084	3								
57			13519.333	-2								

TABLE 1—*Continued*

	0-1				1-2				2-3			
J	R(J)	O-C	P(J)	O-C	R(J)	O-C	P(J)	O-C	R(J)	O-C	P(J)	O-C
1	13261.353	2			13121.527	-3						
2	13265.046	-7	13243.740	-1	13125.270	-0						
3	13268.470	-2	13238.635	-7	13128.764	3	13099.154	4				
4	13271.606	-1	13233.270	3	13132.001	-1	13093.947	0	13037.677	-0	13000.314	2
5	13274.456	-0	13227.617	0	13134.990	1	13088.496	-4	13040.536	1	12994.877	-11
6	13277.026	6	13221.691	-1	13137.719	0	13082.811	-1	13043.133	3	12989.221	10
7	13279.298	1	13215.488	-4	13140.190	1	13076.877	-4	13045.452	-8	12983.286	2
8	13281.284	1	13209.024	5	13142.401	3	13070.706	0	13047.523	1	12977.095	-11
9	13282.973	-6	13202.273	-1	13144.340	-1	13064.290	2	13049.315	-0	12970.677	-0
10	13284.384	1	13195.255	-1	13146.015	1	13057.625	2	13050.837	1	12964.002	3
11	13285.495	2	13187.966	-1	13147.413	-0	13050.715	2	13052.086	2	12957.069	-0
12	13286.310	1	13180.408	2	13148.537	1	13043.553	0	13053.058	1	12949.896	6
13	13286.830	3	13172.576	1	13149.377	-0	13036.143	1	13053.749	-2	12942.459	-1
14	13287.048	2	13164.474	0	13149.931	-2	13028.480	1	13054.010	* -157	12934.778	0
15	13286.964	-2	13156.103	1	13150.192	-6	13020.560	-1	13054.478	* 176	12926.847	1
16	13286.586	3	13147.464	4	13150.162	-7	13012.383	-4	13055.287	* 1132	12918.507	* -156
17	13285.897	-1			13149.777	* -66	13003.948	-5	13053.544	* -182	12910.408	* 179
18	13284.908	2	13129.370	1	13149.232	* 19	12995.246	-11	13052.931	* -86	12902.678	* 1132
19	13283.607	0	13119.918	-0	13148.282	7	12986.227	* -71	13051.984	* -47	12892.436	* -181
20	13281.998	-1	13110.196	-3	13147.030	3	12977.095	* 24	13050.743	* -28	12883.354	* -88
21	13280.080	0	13100.214	3	13145.462	-0	12967.581	6	13049.237	-8	12873.979	* -49
22	13277.847	-0	13089.956	2	13143.576	-1	12957.810	2	13047.466	4	12864.350	* -29
23	13275.292	-9	13079.428	2	13141.368	-1	12947.765	0	13045.452	16	12854.498	-9

TABLE I—*Continued*

	0-1				1-2				2-3			
J	R(J)	O-C	P(J)	O-C	R(J)	O-C	P(J)	O-C	R(J)	O-C	P(J)	O-C
24	13272.441	5			13138.832	-1	12937.448	1	13043.194	8	12844.425	5
25	13269.255	2	13057.558	-5	13135.966	1	12926.847	-2	13040.728	-6	12834.142	7
26	13265.750	0	13046.231	4	13132.760	-2	12915.966	-5			12823.676	4
27	13261.922	-2	13034.623	2	13129.219	-0	12904.806	-4			12813.051	-5
28	13257.766	-5	13022.742	-2	13125.336	1	12893.364	1				
29	13253.292	-1	13010.599	2	13121.108	2	12881.631	2				
30	13284.484	-1	12998.181	3	13116.522	-5	12869.608	1				
31	13243.343	-2	12985.487	-0			12857.298	3				
32	13237.870	-3	12972.523	-2			12844.687	-4				
33	13232.062	-2										
34	13225.919	0	12945.780	-1								
35	13219.434	2	12931.997	-2								
36	13212.606	1	12917.942	-1								
37	13205.429	-3	12903.605	-6								
38	13197.919	7	12889.007	4								
39	13190.048	4	12874.121	2								
40	13181.826	2	12858.961	4								
41	13173.245	-6	12843.512	-4								
42	13164.325	3	12827.798	2								
43	13155.036	2	12811.791	-5								

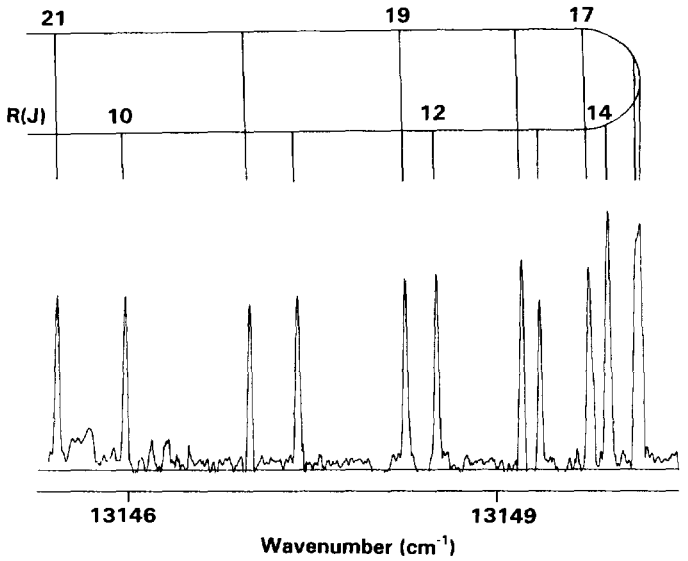

FIG. 1. A portion of the 1–2 band of the $C^1\Sigma^+$–$X^1\Sigma^+$ system of YD near the R head.

The spectrum of YH was first observed by Bernard and Bacis (*25*) in 1976. In a later paper (*26*), these authors reported a rotational analysis of several bands of YH and YD in the 450–900 nm spectral region. Bernard and Bacis (*26*) classified the observed bands into five electronic transitions involving three low-lying states that they called $X^3\Delta$, $A^1\Pi$, and $A'^1\Sigma^+$. On the basis of some primitive ab initio calculations for ScH (*20, 21*), they concluded that the ground state of YH was $X^3\Delta$. This conclusion was inconsistent with a recent theoretical study of YH by Langhoff *et al.* (*14*). These authors studied the low-lying states of YH and predicted a $^1\Sigma^+$ state as the ground state. More recently, Balasubramanian and Wang (*15*) have performed complete active space self consistent field (CASSCF) with second-order configuration interaction (SOCI) and relativistic configuration interaction (RCI) calculations on 29 Ω-states

TABLE II

Spectroscopic Constants (in cm^{-1}) of the $X^1\Sigma^+$ State of YD

Constants	v=0	v=1	v=2	v=3
T_v	0.0	1069.4733(12)	2119.3847(18)	3149.8208(30)
B_v	2.304436(16)	2.271467(15)	2.238506(19)	2.205575(39)
$10^5 \times D_v$	4.2011(20)	4.1903(15)	4.1805(36)	4.182(11)
$10^{10} \times H_v$	6.605(94)	6.626(48)	6.77(21)	7.79(99)
$10^{14} \times L_v$	-1.34(14)	-1.34[b]	-1.34[b]	-1.34[b]

[a]The numbers in parentheses are one standard deviation in the last digit.
[b]Fixed to the value for v=0.

TABLE III

Spectroscopic Constants (in cm^{-1}) of the $C^1\Sigma^+$ State of YD

Constants	v=0	v=1	v=2
T_v	14322.5775(9)	15232.6947(15)	16169.3004(24)
B_v	2.131819(16)	2.116468(17)	2.077765(40)
$10^5 \times D_v$	4.4083(20)	5.4423(30)	4.561(21)
$10^9 \times H_v$	0.7867(91)	4.006(24)	-3.66(43)
$10^{11} \times L_v$	-0.0028(15)	-0.0503(7)	1.060(27)

[a]The numbers in parentheses are one standard deviation in the last digit.

taking into account both electron correlation and spin–orbit effects. This theoretical work also contradicts the $^3\Delta$ assignment of the ground state of YH and YD by Bernard and Bacis (*26*) and, instead, predicts a $^1\Sigma^+$ ground state.

In continuation of a project aimed at increasing the experimental data available for transition metal hydrides, we have recently investigated the electronic spectra of CrH (*27*), H f H, H f D (*28*) and YH (*29*) from the near-infrared to the visible region. For YH, we have analyzed several bands of the $C^1\Sigma^+$–$X^1\Sigma^+$ transition with $v', v'' \leqslant 3$. This study provided a precise determination of the ground state equilibrium constants for this molecule. We have also identified two new electronic transitions, $d0^+(^3\Sigma^-)$–$X^1\Sigma^+$ and $e^3\Phi$–$a^3\Delta$ in the red and near-infrared regions, respectively. Prior to our work, Simard *et al.* (*30*) recorded the laser excitation spectra of YH and YD under

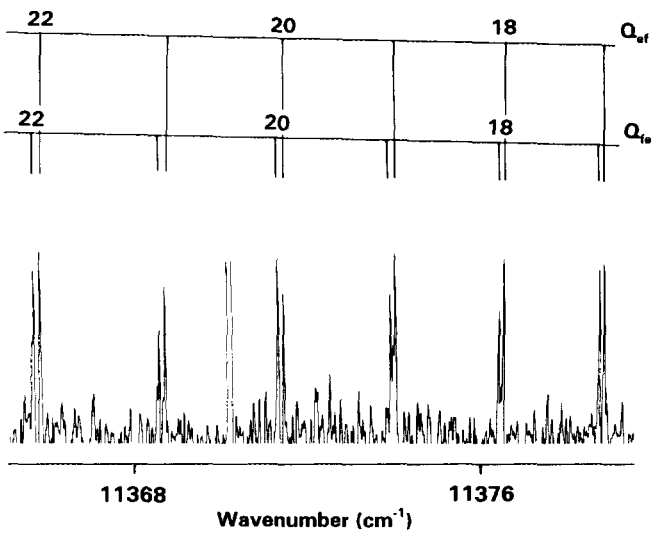

FIG. 2. A portion of the Q branch of the 0–0 band of the $e^3\Phi_2$–$a^3\Delta_1$ subband of YD.

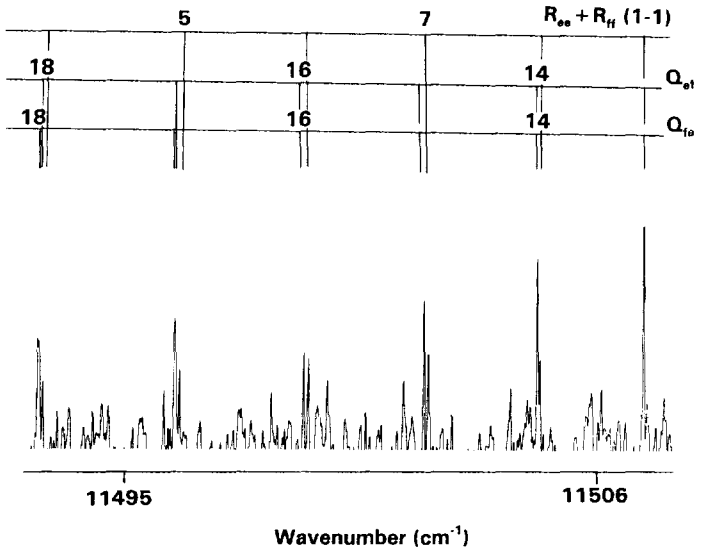

FIG. 3. A portion of the Q branch of the 0–0 band of the $e^3\Phi_3$–$a^3\Delta_2$ subband of YD. Some overlapping lines of the R branch of the 1–1 band have also been marked.

jet-cooled conditions. In addition to the $C^1\Sigma^+$–$X^1\Sigma^+$ transition, they have identified several new electronic transitions in the blue and green regions of the spectrum for YH and YD. This study has also clearly demonstrated that the ground state of these molecules is indeed a $^1\Sigma^+$ state. In the present paper, we report on the red and infrared spectra of the YD molecule to follow our work on YH (*29*). In addition to the strong $C^1\Sigma^+$–$X^1\Sigma^+$ transition, we have identified a new $e^3\Phi$–$a^3\Delta$ transition of YD analogous to the corresponding transition in YH.

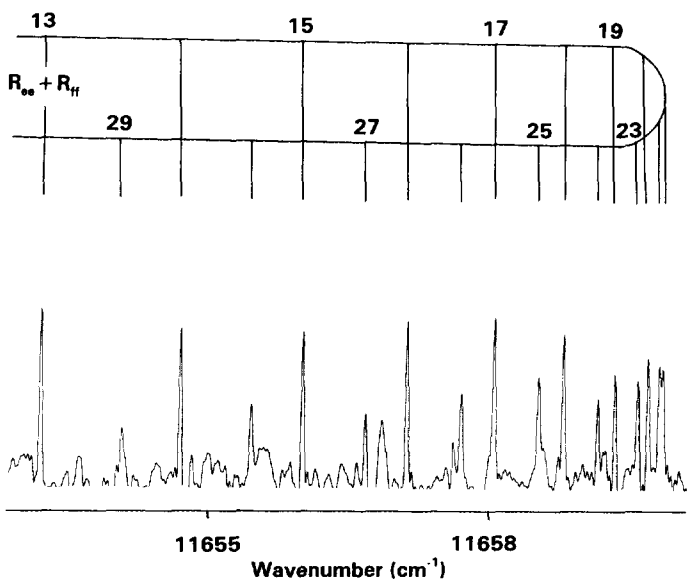

FIG. 4. A portion of the 0–0 band of the $e^3\Phi_4$–$a^3\Delta_3$ subband of YD near the R head.

TABLE IVA

Observed Wavenumbers (in cm^{-1}) of the 0–0 and 1–1 Bands of the $e^3\Phi_2$–$a^3\Delta_1$ Subband of YD

	0-0							
J	Ree	O-C	Rff	O-C	Qef	O-C	Qfe	O-C
3	11413.601	0	11413.601	-5				
4	11417.176	7	11417.176	-3	11396.812	-5	11396.812	5
5	11420.615	6	11420.615	-8	11396.192	-5	11396.192	8
6	11423.926	8	11423.926	-12	11395.447	-7	11395.447	12
7	11427.106	12	11427.106	-13	11394.575	-10	11394.575	15
8	11430.131	-5	11430.176	6	11393.594	3	11393.558	-1
9	11433.041	-2	11433.089	5	11392.470	2	11392.427	-2
10	11435.811	-1	11435.866	4	11391.221	3	11391.171	-1
11	11438.445	3	11438.501	-1	11389.840	1	11389.783	-1
12	11440.930	-2	11441.002	1	11388.331	1	11388.269	2
13	11443.276	-2	11443.360	2	11386.691	1	11386.620	2
14	11445.477	-2	11445.573	1	11384.918	0	11384.836	-1
15	11447.530	-4	11447.640	2	11383.013	0	11382.924	1
16	11449.436	-3	11449.555	-2	11380.969	-4	11380.872	-2
17	11451.193	2	11451.325	-1	11378.797	0	11378.690	0
18	11452.805	7	11452.944	2	11376.484	-0	11376.371	3
19	11454.243	-2	11454.406	2	11374.030	-3	11373.911	1
20	11455.531	-6	11455.713	3	11371.439	-3	11371.312	0
21	11456.671	1	11456.858	1	11368.709	-2	11368.572	-2
22	11457.641	-0	11457.842	-2	11365.837	0	11365.697	2
23	11458.450	-2	11458.671	2	11362.819	-1	11362.678	3
24	11459.100	2	11459.329	-2				
25	11459.581	3	11449.824	-2	11356.355	2	11356.208	1
26					11352.902	1	11352.757	0
27					11349.304	1	11349.159	-4
	1-1							
9	11384.561	1	11384.600	-1				
10	11387.227	-2	11387.283	2	11343.380	5	11343.328	-1
11					11341.960	-0	11341.904	-2
12	11392.140	1	11392.212	-2	11340.414	1	11340.347	-2
13	11394.379	4	11394.462	-3	11338.733	2	11338.658	-1
14					11336.920	4	11336.829	-4
15					11334.965	2	11334.865	-6
16					11332.874	-1	11332.770	-2
17					11330.649	2	11330.537	2
18					11328.279	-2	11328.162	4
19					11325.776	1	11325.638	-3
20					11323.129	1	11322.984	-0
21					11320.338	-1	11320.189	5
22					11317.405	-2	11317.248	5
23					11314.332	2	11314.158	-0
24					11311.106	-5	11310.927	-2
25							11307.558	1
26					11304.236	-0	11304.039	-1
27					11300.584	2	11300.380	-0
28							11296.575	-0

TABLE IVB

Observed Wavenumbers (in cm^{-1}) of the 0–0 and 1–1 Bands of the $e^3\Phi_3$–$a^3\Delta_2$ Subband of YD

	0-0											
J	Ree	O-C	Rff	O-C	Qef	O-C	Qfe	O-C	Pee	O-C	Pff	O-C
2	11534.860	5	11534.860	5								
3	11538.433	2	11538.433	2								
4	11541.829	2	11541.829	2	11521.285	0	11521.285	0				
5	11545.044	2	11545.044	2	11520.397	-4	11520.397	-4				
6	11548.076	1	11548.076	-0	11519.342	-1	11519.342	-0				
7	11550.927	1	11550.927	-1	11518.108	0	11518.108	1				
8	11553.596	1	11553.596	-1	11516.697	-2	11516.697	0				
9	11556.082	2	11556.082	-2					11478.215	2	11478.215	-1
10	11558.382	-0	11558.382	-6	11513.353	-4	11513.353	0	11472.387	4	11472.387	-1
11	11560.501	1	11560.501	-6	11511.422	-4	11511.422	2	11466.390	2	11466.390	-5
12	11562.436	2	11562.436	-8	11509.319	-3	11509.319	5	11460.237	6	11460.237	-4
13	11564.187	3	11564.187	-11	11507.044	-2	11507.044	8	11453.920	7	11453.920	-6
14	11565.750	2	11565.750	-16	11504.592	-7	11504.592	7	11447.441	7	11447.441	-10
15	11567.138	10	11567.138	-13	11501.973	-9	11501.973	8	11440.814	16	11440.814	-6
16	11568.332	10	11568.332	-20	11499.186	-10	11499.186	12	11434.021	16	11434.021	-12
17	11569.324	-8			11496.232	-9	11496.232	19				
18	11570.150	-6	11570.203	3	11493.122	4	11493.083	-2				
19	11570.792	-2	11570.853	5	11489.833	5	11489.787	-1	11412.712	7	11412.755	-1
20	11571.247	0	11571.318	7	11486.376	5	11486.323	-1	11405.311	8	11405.370	5
21	11571.501	-13	11571.595	4	11482.753	3	11482.695	1	11397.760	7	11397.847	21
22	11571.595	-0	11571.687	3	11478.963	-0	11478.911	12	11390.051	-6	11390.150	7
23			11571.595	2	11475.015	3	11474.936	-2			11382.308	-8
24	11571.195	-3	11571.318	2	11470.902	4	11470.813	-1	11374.227	-6	11374.333	-14
25	11570.719	0	11570.853	-1	11466.622	1	11466.524	-3	11366.101	-7		
26	11570.053	-1	11570.203	-3	11462.189	7	11462.079	2				
27	11569.195	-6			11457.580	-2	11457.462	-2				
28	11568.161	0	11568.332	-19	11452.805	-14	11452.696	6				
29	11566.926	-7	11567.138	-4	11447.891	-4						
30	11565.518	3			11442.810	1						
31	11563.913	5			11437.563	1						

TABLE IVB—*Continued*

J	Ree	O-C	Rff	O-C	Qef	O-C	Qfe	O-C	Pee	O-C	Pff	O-C
						1-1						
2	11486.376	1	11486.376	1								
3	11489.878	1	11489.878	1	11473.723	6	11473.723	6				
4	11493.200	2	11493.200	2	11473.008	5	11473.008	5				
5	11496.338	1	11496.338	1	11472.109	-3	11472.109	-3				
6	11499.295	2	11499.295	2	11471.040	-3	11471.040	-3				
7	11502.063	-2	11502.063	-2	11469.791	-6	11469.791	-6				
8	11504.651	-2	11504.651	-2	11468.370	-3	11468.370	-3	11436.105	-0	11436.105	-0
9	11507.044	-12	11507.044	-12	11466.771	-2	11466.771	-2	11430.490	-3	11430.490	-3
10	11509.268	-5	11509.268	-5	11464.996	-0	11464.996	-0	11424.708	-6	11424.708	-6
11	11511.301	-4	11511.301	-4	11463.047	2	11463.047	2	11418.765	-3	11418.765	-3
12	11513.149	-0	11513.149	-0	11460.920	2	11460.920	2	11412.664	5	11412.664	5
13	11514.808	1	11514.808	1	11458.621	3	11458.621	3	11406.397	9	11406.397	9
14	11516.286	9	11516.286	9	11456.149	3	11456.149	3	11399.961	3	11399.961	3
15	11517.569	9	11517.569	9	11453.506	3	11453.506	3	11393.367	-4	11393.367	-4
16	11518.645	-11	11518.645	-11	11450.687	-3	11450.687	-3	11386.630	-2	11386.630	-2
17					11447.702	-8	11447.702	-8				
18					11444.548	-16	11444.548	-16				
19					11441.228	-28	11441.228	-28				
20					11437.787	-0	11437.787	-0				
21					11434.164	2	11434.164	2				

TABLE IVC

Observed Wavenumbers (in cm^{-1}) of the 0–0 and 1–1 Bands of the $e^3\Phi_4$–$a^3\Delta_3$ Subband of YD

	0-0						1-1					
J	Ree+Rff	O-C	Qef+Qfe	O-C	Pee+Pff	O-C	Ree+Rff	O-C	Qef+Qfe	O-C	Pee+Pff	O-C
3	11627.174	1					11577.852	3				
4	11630.599	-1	11609.838	-5			11581.208	5				
5	11633.843	1					11584.366	-8				
6	11636.900	1	11607.868	1			11587.354	-3	11558.817	1		
7	11639.771	2	11606.609	0			11590.154	1	11557.561	5		
8	11642.454	2	11605.172	-0	11572.008	5	11592.763	1	11556.112	-3		
9	11644.947	1	11603.556	0	11566.263	-14	11595.180	-1	11554.494	-0		
10	11647.251	1	11601.761	0	11560.371	-1	11597.409	1	11552.693	1		
11	11649.367	1	11599.786	-0	11554.298	1	11599.444	-1	11550.707	-2		
12	11651.290	0	11597.633	-0	11548.076	22	11601.290	1	11548.543	-4		
13	11653.022	1	11595.299	-1	11541.642	-2	11602.937	-1	11546.202	-1		
14	11654.560	1	11592.783	-6	11535.066	-2	11604.391	-2	11543.676	-1		
15	11655.905	0	11590.098	-0	11528.335	8	11605.653	0	11540.972	0	11480.260	3
16	11657.055	-1	11587.228	-1	11521.425	3	11606.716	2	11538.084	-1	11473.403	-2
17	11658.009	-1	11584.180	-1	11514.355	-0	11607.583	3	11535.019	2	11466.390	2
18	11658.767	-1	11580.954	-1	11507.130	4	11608.250	4	11531.769	-0	11459.204	-3
19	11659.327	-2	11577.550	1	11499.733	-3	11608.716	2	11528.335	-4		
20	11659.691	-0	11573.965	-1	11492.187	1	11608.986	5	11524.733	3		
21	11659.858	3	11570.203	0	11484.477	-1	11609.047	-2	11520.938	-2	11436.689	1
22	11659.816	-3	11566.263	1	11476.613	2	11608.913	-2	11516.965	-3	11428.862	2
23	11659.580	-0	11562.143	1	11468.585	-2	11608.574	-5	11512.819	1	11420.876	3
24	11659.142	2	11557.842	-2	11460.407	0	11608.039	-2	11508.486	-3		
25	11658.498	1	11553.366	-1			11607.309	6	11503.977	-3		
26	11657.649	0	11548.709	-2					11499.295	1		
27	11656.598	2	11543.874	-1								
28	11655.339	3	11538.860	-1								
29	11653.863	-6	11533.665	-1								
30	11652.202	9										
31	11650.301	-6	11522.739	3								

TABLE V

Spectroscopic Constants (in cm^{-1}) of the $a^3\Delta$ Spin Components of YD

	$a^3\Delta_1$		$a^3\Delta_2$		$a^3\Delta_3$	
Constants	v=0	v=1	v=0	v=1	v=0	v=1
T_v	0.0	a	b	c	d	e
B_v	2.09992(11)	2.06788(22)	2.144631(67)	2.11043(17)	2.167713(32)	2.132781(77)
$10^5 \times D_v$	3.241(30)	3.228(64)	4.136(16)	2.53(10)	4.2439(66)	4.190(21)
$10^9 \times H_v$	-0.62(24)	--	0.62(11)	-13.6(20)	0.676(41)	0.71(17)
$10^4 \times q$	4.630(81)	4.379(62)	--	--	--	--
$10^7 \times q_{Dv}$	-2.55(15)	--	3.95(16)	--	--	--
$10^{10} \times q_{Hv}$	--	--	-1.93(21)	--	--	--

Note: (i). The letters a, b, c, d and e represent the undetermined positions of v=1 ($a^3\Delta_1$), v=0 ($a^1\Delta_2$), v=1 ($a^3\Delta_2$), v=0 ($a^3\Delta_3$) and v=1 ($a^3\Delta_3$) vibrational levels relative to v=0 of the $a^3\Delta_1$ spin component, respectively.

(ii). The numbers in parentheses are one standard deviation in the last digit.

EXPERIMENTAL DETAILS

The YD molecule was made in a yttrium hollow cathode lamp. The cathode was prepared by inserting a solid cylindrical rod of yttrium metal into a hole in a copper block. The central part was then bored through to provide a uniform layer of yttrium metal inside the cathode. The lamp was operated at 450 mA current and 220 V current with a slowly flowing mixture of 2.2 Torr of Ne and 50 mTorr of D_2. The emission from the lamp was observed with the 1-m Fourier transform spectrometer associated with the McMath Solar Telescope of the National Solar Observatory.

TABLE VI

Spectroscopic Constants (in cm^{-1}) of the $e^3\Phi$ Spin Components of YD

	$e^3\Phi_2$		$e^3\Phi_3$	
Constants	v=0	v=1	v=0	v=1
T_v	11398.0507(14)	11350.3898(41)+a	11523.0532(13)+b	11474.7871(18)+c
B_v	2.03806(11)	2.00434(24)	2.056156(67)	2.02121(18)
$10^5 \times D_v$	3.676(29)	3.646(69)	3.854(15)	3.37(11)
$10^9 \times H_v$	0.39(23)	0.012(7)	--	-11.0(20)
$10^7 \times q_{Dv}$	-1.101(42)	-2.26(11)	-0.442(34)	--

	$e^3\Phi_4$	
Constants	v=0	v=1
T_v	11611.6396(7)+d	11562.5962(13)+e
B_v	2.077860(32)	2.042813(80)
$10^5 \times D_v$	4.1980(63)	4.259(21)
$10^9 \times H_v$	0.448(37)	1.27(17)

[a]The numbers in parentheses are one standard deviation in the last digit.

TABLE VII

Equilibrium Constants (in cm^{-1}) of the $X^1\Sigma^+$ State of YD

Constants	$X^1\Sigma^+$
ω_e	1089.1182(85)
$\omega_e x_e$	9.8459(38)
$\omega_e y_e$	0.0144(8)
B_e	2.320912(10)
α_e	0.032960(6)
$10^5 \times D_e$	4.2054(19)
$10^7 \times \beta_e$	-0.98(13)
r_e(Å)	1.920404(4)

[a]The numbers in parentheses are one standard deviation in the last digit.

The spectra in the 3500–14800 cm^{-1} spectral region were observed in two experiments. The 3500–9150 cm^{-1} region was recorded using InSb detectors, cold green uranium glass filters, and silicon filters with 10 scans coadded in about 70 min of integration. For the 9100–14 800 cm^{-1} region, the spectrometer was operated with a red-pass filter (RG715) and Si-diode detectors. A total of 10 scans were coadded in 70 min of integration. In both of these experiments, the spectrometer resolution was set at 0.02 cm^{-1}.

In addition to YD bands, the observed spectra also contained Y and Ne atomic lines. The spectra were calibrated using the measurements of the Ne atomic lines made

TABLE VIII

Equilibrium Constants (in cm^{-1}) of the $a^3\Delta$ Spin Components of YD

Constants	$a^3\Delta_1$	$a^3\Delta_2$	$a^3\Delta_3$
B_e	2.11586(17)	2.16173(20)	2.18518(9)
α_e	0.03205(25)	0.03420(18)	0.03493(8)
r_e(Å)	2.01126(8)	1.98985(9)	1.97915(4)

[a]The numbers in parentheses are one standard deviation in the last digit.

TABLE IX

Equilibrium Constants (in cm^{-1}) of the $e^3\Phi$ Spin Components of YD

Constants	$e^3\Phi_2$	$e^3\Phi_3$	$e^3\Phi_4$
B_e	2.05492(17)	2.07363(12)	2.09539(5)
α_e	0.03372(26)	0.03495(19)	0.03505(9)
r_e(Å)	2.04091(8)	2.03168(6)	2.02111(3)

[a]The numbers in parentheses are one standard deviation in the last digit.

by Palmer and Engleman (*31*). The absolute accuracy of the wavenumber scale is expected to be better than ± 0.002 cm^{-1}. The strong lines of YD appear with a typical signal-to-noise ratio of 12:1, and the molecular lines of YD have a typical linewidths of about 0.04 cm^{-1}. For weaker bands, the poor signal-to-noise ratio and blending caused by overlapping lines limit the precision of measurement to ± 0.003 cm^{-1}.

OBSERVATION AND ANALYSIS

The spectral line positions were extracted from the observed spectra using a data reduction program called PC-DECOMP developed by J. Brault. The peak positions were determined by fitting a Voigt lineshape function to each spectral feature. The branches in the different subbands were sorted out using a color Loomis–Wood program running on a PC computer.

The electronic spectrum of YD is expected to be very similar to the spectrum of YH. In our recent work on the electronic spectra of YH (*29*), our data were consistent with a $^1\Sigma^+$ ground state and a $^3\Delta$ state as the first excited state. This result is in agreement with the ab initio calculations (*14, 15*). In the YH work, we relabeled most of the electronic states on the basis of the most recent theoretical (*15*) and experimental (*26, 29*) data available for this molecule. In the present paper, we will adopt the revised notation for YH (*29*) for the different electronic states of YD.

The spectrum of YD consists of two types of bands in the red to the near-infrared region. The bands in the 690 nm–1 μm region are degraded toward lower wavenumbers, while the infrared region bands (1–3 μm) are degraded toward higher wavenumbers. The spectra in these two regions will be discussed separately.

(I) 690 nm to 1 μm Spectral Region

There are several bands of YD in the 11 000–14 500 cm^{-1} spectral region. As in the case of YH, the most intense bands in this region belong to the $C^1\Sigma^+$–$X^1\Sigma^+$ transition. Bernard and Bacis (*26*) have published the rotational analysis of several bands of this transition of YD. In the present work, we have obtained more precise measurements of six bands 0–0, 1–1, 2–2, 0–1, 1–2, and 2–3 of the $C^1\Sigma^+$–$X^1\Sigma^+$ transition. The rotational analysis of these bands provides a set of more accurate molecular constants for YD than that reported earlier.

In our previous work on YH (*29*), we observed several very weak bands in the same region as the $C^1\Sigma^+$–$X^1\Sigma^+$ transition. We assigned these bands to a new $d0^+(^3\Sigma^-)$–$X^1\Sigma^+$ transition. Since the spectrum of YD is much weaker in intensity

than that of YH, we are unable to identify the corresponding $d0^+(^3\Sigma^-)$–$X\,^1\Sigma^+$ transition of YD because of a poor signal-to-noise ratio.

As in the case of YH, we also observe dense structure in the 11 800–13 400 cm^{-1} region of YD. This spectrum seems to be affected by severe perturbations since no pronounced heads or regular branches are obvious. We are unable to assign the spectrum in this region. As pointed out in our YH paper (*29*), a $^1\Pi$–$X\,^1\Sigma^+$ transition is expected to be present in this region and some of the lines could be due to this transition. In addition to these lines, there are some additional very weak and isolated P branches in the 11 500–12 500 cm^{-1} region. These P lines could not be assigned because of the lack of the corresponding R branches. These branches could be due to transitions between two excited states.

To lower wavenumbers, we have observed a new $e^3\Phi$–$a^3\Delta$ transition. Three new bands observed with band origins at 11 398.05, 11 523.05, and 11 611.64 cm^{-1} have been identified as the respective 0–0 bands of the $^3\Phi_2$–$^3\Delta_1$, $^3\Phi_3$–$^3\Delta_2$, and $^3\Phi_4$–$^3\Delta_3$ subbands of the $e^3\Phi$–$a^3\Delta$ transition. These bands are followed to lower wavenumbers by relatively weaker 1–1 bands associated with each subband.

(i) The $C^1\Sigma^+$–$X^1\Sigma^+$ transition. We have observed the bands of the $\Delta v = 0$ and $\Delta v = -1$ sequences of the $C^1\Sigma^+$–$X^1\Sigma^+$ transition. Some of these bands were also studied by Bernard and Bacis (*26*). The structure of each band consists of a single R and a single P branch as expected for a $^1\Sigma^+$–$^1\Sigma^+$ transition. As observed in the case of YH, the lines of the P branch are stronger than the R branch by at least a factor of 2.

The band with an R head at 14 350.6 cm^{-1} is the strongest band of this system and has been assigned as the 0–0 band. We have observed the structure of this band up to $R(56)$ and $P(57)$. This band is free from local perturbations. The 0–1 band of this transition is also free from perturbation and we are able to identify lines up to $R(43)$ and $P(43)$ in this band.

Except for the 0–0 and 0–1 bands, the other bands involving $v' = 1$ and $v' = 2$ are perturbed by unknown close-lying states. In the 1–1 band, we have observed transitions involving J up to $J' = 42$. The excited $v' = 1$ vibrational level is perturbed in two regions, one at $J' = 18$ and the other at $J' = 32$. The $J' = 18$ perturbation can be clearly seen in the 1–2 band (see Table I), but the high-J lines of this band could not be identified.

Our spectra consist of two bands, 2–2 and 2–3, with $v' = 2$. The lines corresponding to a maximum $J' = 28$ could be identified in these bands. The $v' = 2$ vibrational level of YD is perturbed at $J' = 17$. This perturbation shifts the corresponding R and P lines by $+1.13$ cm^{-1} with respect to their predicted positions. Several lines in the perturbation region were not directly included in the determination of the molecular constants, although the ground state combination differences corresponding to the perturbed transitions were included in the determination of the ground state rotational constants. A part of the spectrum of the 1–2 band of this transition near the R head is provided in Fig. 1.

The observed line positions were fitted to the following customary energy level expression for each vibrational level of a $^1\Sigma^+$ state:

$$F_v(J) = T_v + B_vJ(J+1) - D_v[J(J+1)]^2 + H_v[J(J+1)]^3 + L_v[J(J+1)]^4. \quad (1)$$

The observed line positions in the different bands of this transition of YD are provided in Table I, and the constants obtained for the $X\,^1\Sigma^+$ and $C^1\Sigma^+$ states are provided in Tables II and III. The molecular parameters T_v, B_v, D_v, H_v, and L_v have been determined for both the states, keeping the term value for $v = 0$ (T_0) fixed to zero. For the

ground state, the L_v parameters were determined only for the $v = 0$ vibrational level and the other values were fixed to L_0. For the $C^1\Sigma^+$ state, all the constants in Eq. (1) were determined. It can be noted (Table III) that the L_v values in the $C^1\Sigma^+$ state increase rapidly with increasing v. This undoubtedly is a reflection of the interaction of the C state with nearby states.

(ii) The $e^3\Phi$–$a^3\Delta$ transition. In this work, we report the first observation of the $e^3\Phi$–$a^3\Delta$ transition of YD analogous to the corresponding transition observed previously in YH (*29*). The assignment of three bands with R heads at 11 460, 11 572, and 11 660 cm^{-1} as the 0–0 bands of the $^3\Phi_2$–$^3\Delta_1$, $^3\Phi_3$–$^3\Delta_2$, and $^3\Phi_4$–$^3\Delta_3$ subbands of the $e^3\Phi$–$a^3\Delta$ transition have been confirmed by rotational analysis.

A part of the spectrum of the 0–0 band of the $^3\Phi_2$–$^3\Delta_1$ subband showing some Q-branch lines is presented in Fig. 2. This subband is the weakest of the three subbands. The P-branch lines of this subband are very weak in intensity and could not be measured. We have, therefore, used only R and Q branches in the determination of molecular constants. The 1–1 band of this subband is even weaker in intensity than the 0–0 band. Even so, we have been able to identify several R and Q lines of this band. The lines of this subband are split into two components due to Ω-doubling effects, present almost entirely in the $a^3\Delta_1$ spin component.

The next higher wavenumber band with an R head at 11 572 cm^{-1} has been identified as the $^3\Phi_3$–$^3\Delta_2$ subband of the $e^3\Phi$–$a^3\Delta$ transition of YD. In this band, the first member of the R branch has been clearly observed, confirming the present Ω-assignments. The high-J lines with $J > 17$ of this band are also split into two components due to a small Ω-doubling effect in the $a^3\Delta_2$ spin component. In 1–1 band of this subband, the high-J lines with resolved Ω-splitting could not be identified due to their weak intensity so that the Ω-doubling constants for $v = 1$ of this subband could not be determined. A part of the Q branch of this band is presented in Fig. 3.

To even higher wavenumbers, a band with an R head at 11 660 cm^{-1} has been assigned as the 0–0 band of the $^3\Phi_4$–$^3\Delta_3$ subband. This subband is the strongest of the three subbands of the $e^3\Phi$–$a^3\Delta$ transition. The P, Q, and R branches of this band do not show any splitting even at high J values, indicating that the Ω-doubling effects in the $e^3\Phi_4$ and $a^3\Delta_3$ spin components are negligible, as expected. A part of the spectrum of this subband near the R head is presented in Fig. 4.

Each subband of the $e^3\Phi$–$a^3\Delta$ transition consists of only P, Q, and R branches and no satellite branches or transitions with $\Delta\Sigma \neq 0$ between the spin components have been observed. Due to lack of satellite branches, we could not determine a single set of the molecular constants for the ground and excited states of YD by treating these states as Hund's case (a) states. Rather than fitting the observed transition wavenumbers with assumed values of A_v and λ_v, we chose to determine the rotational constants in each spin component separately. The observed line positions in different subbands were fitted using the following Hund's case (c) expression:

$$F_v(J) = T_v + B_vJ(J+1) - D_v[J(J+1)]^2 + H_v[J(J+1)]^3 \pm 1/2\{q(J(J+1) + q_D[J(J+1]^2 + q_H[J(J+1)]^3\}. \quad (2)$$

We have measured the rotational structure in the 0–0 and 1–1 bands of each subband and have determined the rotational constants for the $v = 0$ and the $v = 1$ vibrational levels of each spin component of both the electronic states. No rotational perturbations have been observed in the analyzed bands of each subband. The observed transition wavenumbers in each subband are provided in Tables IVA–IVC, and the molecular

constants for the $a^3\Delta$ and $e^3\Phi$ states are provided in Tables V and VI, respectively. Since the resolved Ω-splitting in the 0–0 and 1–1 bands of the $e^3\Phi_2$–$a^3\Delta_1$ subband and the 0–0 band of the $e^3\Phi_3$–$a^3\Delta_2$ subband was resolved, we have been able to determine the Ω-doubling constants in these spin components.

The e/f parity assignment is difficult. Following the YH analysis (*29*), we chose to put the e parity level above the f parity level for a given J in the $a^3\Delta_1$ and $a^3\Delta_2$ spin components.

(II) 1–3 μm Spectral Region

Several violet-degraded $\Delta\Omega = 0$ bands have been identified in this spectral region with P heads at 7822.0, 7869.5, 7895.5, 7907.7, and 8005.6 cm^{-1}. The first four bands consist of a single pair of P and R branches, while the lines of the band with the P head at 8005.6 cm^{-1} consist of two P and two R branches. The splitting in the branches of this band arise, presumably, from Ω-doubling. These bands are, however, very weak in intensity and the low-J lines could not be identified because of the very small signal-to-noise ratio (4:1) for the strong lines.

The band at 7822 cm^{-1} seems to be the 0–0 band of a new electronic transition. In addition to the poor signal-to-noise, the major problem with the analysis of these bands is that the standard deviation of the fit is not sensitive to changes in the J-assignments. This creates an uncertainty in the J-assignments of at least ± 2 units. Therefore, in the 0–0 band, we chose a J-assignment based on the magnitude of the centrifugal distortion constants. Using this approach, we obtained the following constants for the 0–0 band with the P head at 7822 cm^{-1}: $T_{0,0} = 7855.1610$ cm^{-1}, $B'_0 = 2.46895$ cm^{-1}, $D'_0 = 1.963 \times 10^{-5}$ cm^{-1}, $B''_0 = 2.30087$ cm^{-1}, and $D''_0 = 2.922 \times 10^{-5}$ cm^{-1}. The rotational constants of the lower and the excited state do not agree with the constants of any known states (even after changing the J-numbering by ± 1 or ± 2). This indicates that most probably two unknown excited states are involved.

The electronic state assignment of these bands is even more uncertain. The heads at 7869.5, 7895.5, and 7907.7 cm^{-1} could be the 1–1, 2–2, and 3–3 bands associated with the 7822 cm^{-1} band. An other possibility is that some of these bands are actually subbands of a transition involving states with a high multiplicity and large Ω-values. The observation of Ω-splitting in the 8005.6 cm^{-1} band supports this possibility. In order to obtain a definite rotational and electronic assignment of these bands, improved spectra with a larger signal-to-noise ratio are required.

DISCUSSION

The rotational constants of individual vibrational levels in the ground $X^1\Sigma^+$ state have been used to evaluate the equilibrium molecular constants provided in Table VII. The equilibrium constants of YD [$\omega_e = 1089.1182(85)$ cm^{-1}, $B_e = 2.320912(10)$ cm^{-1}] can be used in the isotopic relationships (*32*), $\omega_e^i = \rho\omega$ and $B_e^i = \rho^2 B_e$ with $\rho^2 = [\mu/\mu^i]$ to test for consistency. The calculated values for YH using the equilibrium constants of YD are $\omega_e = 1531.11$ cm^{-1} and $B_e = 4.5869$ cm^{-1} which can be compared with the experimental values (*29*) [$\omega_e = 1530.456(15)$ cm^{-1}, $B_e = 4.575667(38)$ cm^{-1}]. The equilibrium rotational constants in the ground state have been used to evaluate the equilibrium bond length. The observed equilibrium bond length of 1.920404(4) Å for YD compares with 1.922765(8) Å obtained for the ground state of YH.

The vibrational intervals $\Delta G(v + 1/2)$ and rotational constants B'_v of the $C^1\Sigma^+$

state of YH are found to vary in an erratic manner (*29*). A similar behavior is observed for the $\Delta G(v + 1/2)$ values of YD. The $\Delta G(3/2)$ value of 936.6057(28) cm^{-1} is larger than the $\Delta G(1/2)$ value, which is 910.1171(18) cm^{-1}. The variation of B'_v with v for YD is not as erratic as found for YH (for YH B'_1 was larger than B'_0). The B values of the $v = 0$, 1, and 2 vibrational levels of YD are 2.131819(16), 2.116468(17), and 2.077765(40) cm^{-1}, respectively. This irregular behavior of the B_v and the $\Delta G(v + 1/2)$ intervals is a result of a strong interaction between the $C^1\Sigma^+$ state a nearby perturbing state (or states). For YH, a $d0^+(^3\Sigma^-)$ state, located about 1460 cm^{-1} above the $v = 0$ level of the $C^1\Sigma^+$ state, has been identified. The perturbations in the $v = 1$ and $v = 2$ vibrational levels of YD could be caused either by the unobserved $d0^+(^3\Sigma^-)$ or $d1(^3\Sigma^-)$ states. Because of the irregular variation with v of the vibrational intervals and rotational constants of the $C^1\Sigma^+$ state, it is difficult to obtain meaningful values for the equilibrium constants for the $C^1\Sigma^+$ state.

CONCLUSION

We have observed the high-resolution emission spectrum of YD molecule using a Fourier transform spectrometer. In addition to the previously known $C^1\Sigma^+$–$X^1\Sigma^+$ transition, we have identified a new $e^3\Phi$–$a^3\Delta$ electronic transition in the near infrared. The rotational analysis of six bands of the $C^1\Sigma^+$–$X^1\Sigma^+$ system provides a much improved set of equilibrium constants for the ground state. The bands of the new $e^3\Phi$–$a^3\Delta$ transition are free from local perturbations. The rotational analysis of the 0–0 and 1–1 bands of this transition provides effective equilibrium rotational constants for the different spin components of the $a^3\Delta$ and $e^3\Phi$ states (see Tables VIII and IX).

ACKNOWLEDGMENTS

We thank J. Wagner, C. Plymate and P. Hartmann of the National Solar Observatory for assistance in obtaining the spectra. The National Solar Observatory is operated by the Association of Universities for Research in Astronomy, Inc., under contract with the National Science Foundation. The research described here was supported by funding from the Petroleum Research Fund, administered by the American Chemical Society, and the NASA Origin of the Solar System program. Support was also provided by the Natural Sciences and Engineering Research Council of Canada. We also thank W. J. Balfour and B. Simard for helpful discussions and for communicating their results prior to publication.

RECEIVED: November 22, 1994

REFERENCES

1. C. J. CHEETHAM AND R. F. BARROW, *Adv. High Temp. Chem.* **1**, 7–41 (1967).
2. R. E. SMITH, *Proc. R. Soc. London A* **332**, 113–127 (1973).
3. P. R. SCOTT AND W. G. RICHARDS, *Chem. Soc. Spec. Period. Rep.* **4**, 70 (1976).
4. P. B. ARMENTROUT AND L. S. BEAUCHAMP, *Acc. Chem. Res.* **22**, 315–321 (1989).
5. P. B. ARMENTOUT AND L. S. SUNDERLIN, *in* "Transition Metal Hydrides" (A. Dedieu, Ed.), pp. 1–64, VCH, NY, 1992.
6. A. D. MCLEAN, *J. Chem. Phys.* **79**, 3392–3402 (1983).
7. P. J. HAY AND R. L. MARTIN, *J. Chem. Phys.* **83**, 5174–5181 (1985).
8. S. P. WALCH AND C. W. BAUSCHLICHER, *J. Chem. Phys.* **78**, 4597–4605 (1983).
9. C. W. BAUSCHLICHER AND S. R. LANGHOFF, *in* "Transition Metal Hydrides" (A. Dedieu, Ed.), pp. 103–127, VCH, NY, 1992.
10. S. W. WANG AND K. S. PITZER, *J. Chem. Phys.* **79**, 3851–3858 (1983).
11. H. BASCH AND S. J. TOPIAL, *J. Chem. Phys.* **71**, 802–814 (1979).
12. P. S. BAGUS AND C. BJÖKMAN, *Phys. Rev. A* **23**, 461–472 (1981).
13. K. BALASUBRAMANIAN, P. Y. FENG, AND M. Z. LIAO, *J. Chem. Phys.* **87**, 3981–3985 (1987).

14. S. R. LANGHOFF, L. G. M. PETTERSSON, C. W. BAUSCHLICHER, AND H. PARTRIDGE, *J. Chem. Phys.* **86,** 268–278 (1987).
15. K. BALASUBRAMANIAN AND J. Z. WANG, *J. Mol. Spectrosc.* **133,** 82–89 (1989).
16. K. BALASUBRAMANIAN AND J. Z. WANG, *Chem. Phys. Lett.* **154,** 525–530 (1989).
17. K. BALASUBRAMANIAN AND J. LI, *J. Phys. Chem.* **94,** 4415–4419 (1990).
18. J. ANGLADA, P. J. BRUNA, AND S. D. PEYERIMHOFF, *Mol. Phys.* **69,** 281–303 (1990).
19. J. ANGLADA, P. J. BRUNA, AND S. D. PEYERIMHOFF, *Mol. Phys.* **66,** 541–563 (1989).
20. P. R. SCOTT AND W. G. RICHARDS, *J. Phys. B* **7,** 1679–1682 (1974).
21. A. B. KUNZE, M. P. GUSE, AND R. J. BLINT, *J. Phys. B* **8,** L358–L361 (1975).
22. R. YERLE, *Astron. Astrophys.* **73,** 346–351 (1979).
23. D. L. LAMBERT AND E. A. MALLIA, *Mon. Not. R. Astron. Soc.* **151,** 437–447 (1971).
24. O. ENGVOLD, H. WÖHL, AND J. W. BRAULT, *Astron. Astrophys. Suppl.* **42,** 209–213 (1980).
25. A. BERNARD AND R. BACIS, *C. R. Acad. Sci. Ser. B* **283,** 339–341 (1976).
26. A. BERNARD AND R. BACIS, *Can. J. Phys.* **55,** 1322–2334 (1977).
27. R. S. RAM, C. N. JARMAN, AND P. F. BERNATH, *J. Mol. Spectrosc.* **161,** 445–454 (1993).
28. R. S. RAM AND P. F. BERNATH, *J. Chem. Phys.* **101,** 74–80 (1994).
29. R. S. RAM AND P. F. BERNATH, *J. Chem. Phys.* **101,** 9283–9288 (1994).
30. B. SIMARD, W. J. BALFOUR, H. NIKI, AND P. A. HACKETT, Abstracts RC11 and RC12 from the 45th Ohio State University Symposium on Molecular Spectroscopy, Columbus, OH, June 11–25, 1990; also, B. SIMARD AND W. J. BALFOUR, private communication.
31. B. A. PALMER AND R. ENGLEMAN, "Atlas of the Thorium Spectrum," Los Alamos National Laboratory, Los Alamos, NM, 1983, unpublished.
32. G. HERZBERG, "Molecular Spectra and Molecular Structure, I. Spectra of Diatomic Molecules," Van Nostrand-Reinhold, NY, 1950.